ETH Zürich

Seminar for Applied Mathematics

D-MATH

Spring semester 2018

Term Project

Low-Frequency Stabilized Electric Field Integral Equation

Lorenzo Giacomel

supervised by

Prof. Dr. Ralf Hiptmair

ETH

Eidgenössische Technische Hochschule Zürich
Swiss Federal Institute of Technology Zurich

Declaration of originality

The signed declaration of originality is a component of every semester paper, Bachelor's thesis, Master's thesis and any other degree paper undertaken during the course of studies, including the respective electronic versions.

Lecturers may also require a declaration of originality for other written papers compiled for their courses.

I hereby confirm that I am the sole author of the written work here enclosed and that I have compiled it in my own words. Parts excepted are corrections of form and content by the supervisor.

Title of work (in block letters):

Low-Frequency Stabilized Electric Field Integral Equation

Authored by (in block letters):

For papers written by groups the names of all authors are required.

Name(s):	**First name(s):**
Giacomel	Lorenzo

With my signature I confirm that

- I have committed none of the forms of plagiarism described in the 'Citation etiquette' information sheet.
- I have documented all methods, data and processes truthfully.
- I have not manipulated any data.
- I have mentioned all persons who were significant facilitators of the work.

I am aware that the work may be screened electronically for plagiarism.

Place, date	**Signature(s)**
Zürich, 15.05.2018	Lorenzo Giacomel

For papers written by groups the names of all authors are required. Their signatures collectively guarantee the entire content of the written paper.

Contents

1 Introduction

The computation of the electric field scattered by a body is a typical problem in electromagnetism. The space can be considered as divided into two regions: the scatterer Ω_s and the free space Ω'. Moreover we have the surface $\Gamma = \partial\Omega$. The analytical solution is known only for very simple geometries, therefore for more realistic cases it is strictly necessary to use computationally intensive numerical methods. We use the Boundary Element Method, which allows to compute the electric field in the whole space, by discretizing only the surface of the scatterer. We deal with time-harmonic quantities, which are of the form

$$\tilde{\mathbf{F}}(x, y, z, t) = \mathbf{F}(x, y, z)e^{i\omega t}.$$

In this case, the Maxwell's equations can be simplified resulting in

$$\begin{cases} \text{div}\mathbf{E} = \frac{\rho}{\varepsilon}, \\ \text{div}\mathbf{H} = 0, \\ \mathbf{curlE} = -i\omega t\mathbf{H}, \\ \mathbf{curlH} = \varepsilon i\omega t\mathbf{E}. \end{cases}$$

Moreover, if we consider a scatterer which is a Perfect Electric Conductor (PEC) hit by an electromagnetic wave $(\mathbf{E}^i, \mathbf{H}^i)$ and if we impose the Sommerfeld radiation conditions, we obtain the following boundary value problem:

$$\begin{cases} \mathbf{curlcurlE} - \kappa^2\mathbf{E} = 0 \quad \text{in } \Omega_s \cup \Omega', \\ \gamma_{\mathbf{t}}\mathbf{E} = -\gamma_{\mathbf{t}}\mathbf{E}^i \quad \text{on } \Gamma, \\ \|\mathbf{curlE} \times \frac{\mathbf{x}}{|\mathbf{x}|} + i\omega\varepsilon\mathbf{E}\|_2 = \mathcal{O}\left(\frac{1}{\|\mathbf{x}\|^2}\right) \quad \text{for } |\mathbf{x}| \to \infty, \end{cases}$$

with $\kappa = \omega\sqrt{\varepsilon\mu}$.
In section 2 we report some useful tools from functional analysis for the derivation of the Boundary Integral Equations (BIEs), which can be found in section 3. We focus on the indirect approach, which is known to lead to an instable formulation when $\kappa \to 0$. Therefore, we use an augmented formulation that is not affected by the low-frequency instability. In section 4 we provide the Boundary Element Spaces used to discretize the BIEs and we show that the discretization leads to simple linear systems. In section 5 we prove that both the continuous and the discrete versions of the augmented formulation are well-posed, using the theory for the saddle-point problems. Finally, in section 6 we report the results we get from our C++ implementation, using the BETL library. We focus on the validation of the code in the simple case of a sphere hit by a plane wave. In this case the Electric field has an analytical form, known as Mie Solution. Moreover, we show that the augmented formulation is stable even when the classical one is not. To conclude, we report also the results of the scattering by a cube, which is a more critical scenario, given that the surface is not smooth.

2 Function Spaces and Traces

The tools from functional analysis are fundamental to derive and analyze the equations which arise in electromagnetic scattering problems. In this section we give a brief overview of the function spaces and the traces used in the following sections. All the results from this section have been more rigorously analyzed and proved in [3].

2.1 Sobolev spaces in the domain and on the boundary

We use the Sobolev spaces H^s_{loc} and $\boldsymbol{H}^s_{\text{loc}}$ for scalar and vector-valued functions respectively, as defined in [5]. Moreover, given a domain $\Omega \subseteq \mathbb{R}^3$ and a first order differential operator $\mathbf{d}$, we define the spaces

$$\boldsymbol{H}^s_{\text{loc}}(\mathbf{d}, \Omega) = \{\mathbf{u} \in \boldsymbol{H}^s_{\text{loc}}(\Omega) : \mathbf{du} \in \boldsymbol{H}^s_{\text{loc}}\},$$
$$\boldsymbol{H}^s_{\text{loc}}(\mathbf{d}0, \Omega) = \{\mathbf{u} \in \boldsymbol{H}^s_{\text{loc}}(\Omega) : \mathbf{du} = 0\}.$$

In case Ω is bounded, we can drop the $_{\text{loc}}$ sub-fix and the $\boldsymbol{H}^s(\Omega)$ spaces are endowed with the norm

$$\|\mathbf{u}\|^2_{\boldsymbol{H}^s(\mathbf{d},\Omega)} := \|\mathbf{u}\|^2_{\boldsymbol{H}^s(\Omega)} + \|\mathbf{du}\|^2_{\boldsymbol{H}^s(\Omega)}$$

and the seminorm

$$|\mathbf{u}|^2_{\boldsymbol{H}^s(\mathbf{d},\Omega)} := |\mathbf{u}|^2_{\boldsymbol{H}^s(\Omega)} + |\mathbf{du}|^2_{\boldsymbol{H}^s(\Omega)}\,.$$

Moreover, the notion of Sobolev space can be extended to spaces of functions defined on Γ. This can be done by using local charts of the manifold Γ. Those spaces are denoted by $\boldsymbol{H}^s(\Gamma)$, $s \in [-1, 1]$, with $\boldsymbol{H}^{-s}(\Gamma)$ being the dual of $\boldsymbol{H}^s(\Gamma)$.

2.2 Traces

When deriving the BIEs for electromagnetic scattering, a crucial role is played by the trace functions. Among all of them, we will only use the tangential trace, the normal trace and the Neumann trace:

$$\gamma_{\mathbf{t}}\mathbf{u} = \mathbf{n} \times \mathbf{u}_{|\Gamma},$$
$$\gamma_{\mathbf{t}}\mathbf{u} = \mathbf{n} \cdot \mathbf{u}_{|\Gamma},$$
$$\gamma_N = \mathbf{curl}\ \mathbf{u}_\Gamma \times \mathbf{n}.$$

A more complete list of traces can be found in [11].
Having in mind the goal of deriving BIEs, we need to identify a proper trace space "$X(\Gamma)$" of $\boldsymbol{H}(\mathbf{curl}, \Omega)$.
According to [3], $X(\Gamma)$ has to meet two requirements:

1. The inner product on $X(\Gamma)$ has an intrinsic definition that does not rely on the embedding of Γ into $\mathbb{R}^3$, i.e. $X(\Gamma)$ should have an interpretation as sections of the tangent bundle to $T\Gamma$ of Γ.

2. $\gamma_{\mathbf{t}} : \boldsymbol{H}(\mathbf{curl}, \Omega) \to X(\Gamma)$ is continuous and surjective.

An important remark is that for the rest of this section we rely on the boundedness of Ω, but the results remain valid also for unbounded Ω.
In order to be as general as possible, we consider the case of Γ being a piecewise smooth domain. It is easy to understand that this case inherently poses additional difficulties, since even if $\mathbf{u} \in \boldsymbol{C}^\infty(\Omega)$ we do not have $\gamma_{\mathbf{t}} \in \boldsymbol{H}^{\frac{1}{2}}$, as the tangential trace is discontinuous across edges of Γ. To tackle these issues, we introduce a new class of Hilbert spaces (as defined in [3]) which play a central role in the definition of the trace space:

Definition 1. *We introduce the Hilbert space* $\boldsymbol{H}^s_\times(\Gamma) := \gamma_{\mathbf{t}}(\boldsymbol{H}^{s+\frac{1}{2}}(\Omega))$, $s \in (0,1)$, *equipped with an inner product that renders* $\gamma_{\mathbf{t}} : \boldsymbol{H}^{s+\frac{1}{2}}(\Omega) \to \boldsymbol{H}^s_\times(\Gamma)$ *continuous and surjective. Its dual space with respect to the pairing*

$$\langle \boldsymbol{\mu}, \boldsymbol{\eta} \rangle_{\boldsymbol{\tau},\Gamma} = \int_\Gamma (\boldsymbol{\mu} \times \mathbf{n}) \cdot \boldsymbol{\eta} \mathrm{d}S$$

is denoted by $\boldsymbol{H}^{-s}_\times(\Gamma)$

As stated in [3] this definition solves the problem of the tangential trace since it can be proved that $\gamma_{\mathbf{t}} : \boldsymbol{H}(\mathbf{curl}, \Omega) \to \boldsymbol{H}^{-\frac{1}{2}}_\times(\Gamma)$ is a linear and continuous mapping. Unfortunately, we still do not have surjectivity, so we have to develop further this theory.
We can define for $\mathbf{u} \in C^\infty(\overline{\Omega})$:

$$\mathrm{div}_\Gamma \gamma_{\mathbf{t}} \mathbf{u} := \begin{cases} \mathrm{div}_j(\gamma_{\mathbf{t}}\mathbf{u})^j & \text{on } \Gamma^j \\ \left((\gamma_{\mathbf{t}}\mathbf{u})^j \cdot \boldsymbol{\nu}^{ij} + (\gamma_{\mathbf{t}}\mathbf{u})^i \cdot \boldsymbol{\nu}^{ij}\right) \delta_{ij}, & \text{on } \overline{\Gamma^j} \cap \overline{\Gamma^i}, \end{cases}$$

where δ_{ij} is the is the delta distribution whose support is the edge $\overline{\Gamma^j} \cap \overline{\Gamma^i}$, div_j denotes the 2D-divergence computed on the face Γ_j and $\boldsymbol{\nu}_{ij}$ is the outer normal to Γ_i restricted to the edge $\overline{\Gamma^j} \cap \overline{\Gamma^i}$. This definition can be extended by a density argument to functionals on $\boldsymbol{H}^{-\frac{1}{2}}_\times$. Now by defining

$$\boldsymbol{H}^{-\frac{1}{2}}_\times(\mathrm{div}_\Gamma, \Gamma) := \{\boldsymbol{\mu} \in \boldsymbol{H}^{-\frac{1}{2}}_\times(\Gamma), \mathrm{div}_\Gamma \boldsymbol{\mu} \in H^{-\frac{1}{2}}(\Gamma)\}$$

we can state the final theorem stated in [3] which shows that this is exactly the space we were looking for:

Theorem 1. *The operator* $\gamma_{\mathbf{t}} : \boldsymbol{H}(\mathbf{curl}, \Gamma) \to \boldsymbol{H}^{-\frac{1}{2}}_\times(\mathrm{div}_\Gamma, \Gamma)$ *is continuous, surjective and possesses a continuous right inverse.*

Proof. The proof in the general case of Lipschitz domains can be found in [2, Theorem 4.1]. □

Besides $\boldsymbol{H}^{-\frac{1}{2}}_\times(\mathrm{div}_\Gamma, \Gamma)$, it is useful to define one more trace space:

$$\boldsymbol{H}^{-\frac{1}{2}}_\perp(\mathbf{curl}_\Gamma, \Gamma) := \{\boldsymbol{\mu} \in \boldsymbol{H}^{-\frac{1}{2}}(\Gamma), \mathbf{curl}_\Gamma \boldsymbol{\mu} \in H^{-\frac{1}{2}}(\Gamma)\}.$$

This space is linked to $\boldsymbol{H}^{-\frac{1}{2}}_\times(\mathrm{div}_\Gamma, \Gamma)$ by a precise relation, which is summarized by the next theorem

Theorem 2. *The mapping*

$$\mathbf{R} : \boldsymbol{H}_{\times}^{-\frac{1}{2}}(\mathrm{div}_{\Gamma}, \Gamma) \longrightarrow \boldsymbol{H}_{\perp}^{-\frac{1}{2}}(\mathbf{curl}_{\Gamma}, \Gamma),$$

defined as $\mathbf{Ru} = \mathbf{u} \times \mathbf{n}$*, is bijective and isometric.*

The usefulness of $\boldsymbol{H}_{\perp}^{-\frac{1}{2}}(\mathbf{curl}_{\Gamma}, \Gamma)$ and $\mathbf{R}$ will be clear in subsection 4.3.

3 EFIE and Augmented EFIE

In this section we derive the Electric Field Boundary Integral Equation (EFIE). Given that this BIE is unstable for low frequencies, we report an augmented formulation which is solvable also for $\kappa \to 0$. The section is structured as follows: first we show the main representation formula for a Maxwell solution, then we introduce the necessary Boundary Integral Operators (BIOs) and, finally, we derive the EFIE.

3.1 Representation Formula

First of all, we define a Maxwell solution.

Definition 2. *A distribution* $\mathbf{e} \in \boldsymbol{H}_{\text{loc}}(\mathbf{curl}^2, \Omega)$ *is called a Maxwell solution on some generic domain* Ω*, if it satisfies the Electric Wave Equation* $\mathbf{curlcurle} - \kappa^2 \mathbf{e} = 0$ *in* Ω *and the Silver-Müller radiation conditions at* ∞*, if* Ω *is not bounded.*

Now, we need to define the potentials related to the Maxwell problem. To do so we will use the fundamental solution of the Helmoltz equation

$$E_\kappa(\mathbf{x}) := \frac{\exp(i\kappa|\mathbf{x}|)}{4\pi|\mathbf{x}|} \quad \text{for } \mathbf{x} \neq 0.$$

Definition 3. *The scalar and vectorial Helmoltz single layer potentials are respectively denoted by* Ψ_V^κ *and* $\boldsymbol{\Psi}_{\boldsymbol{V}}^\kappa$ *and they are defined as*

$$\Psi_V^\kappa(\phi)(\mathbf{x}) := \int_\Gamma \phi(\mathbf{x}) E_\kappa(\mathbf{x} - \mathbf{y}) dS(\mathbf{x}),$$
$$\boldsymbol{\Psi}_{\boldsymbol{V}}^\kappa(\boldsymbol{\mu})(\mathbf{x}) := \int_\Gamma \boldsymbol{\mu}(\mathbf{x}) E_\kappa(\mathbf{x} - \mathbf{y}) dS(\mathbf{x}),$$

for $\mathbf{x} \notin \Gamma$.

Moreover, we need to define some layer potentials which are used exclusively for the case of the Maxwell equations.

Definition 4. *The Maxwell single layer and double layer potentials are respectively denoted by* $\boldsymbol{\Psi}_{SL}^\kappa$ *and* $\boldsymbol{\Psi}_{DL}^\kappa$ *and they are defined as*

$$\boldsymbol{\Psi}_{SL}^\kappa(\boldsymbol{\mu})(\mathbf{x}) := \kappa \boldsymbol{\Psi}_{\boldsymbol{V}}^\kappa(\boldsymbol{\mu})(\mathbf{x}) + \frac{1}{\kappa} \mathbf{grad}_{\mathbf{x}} \boldsymbol{\Psi}_{\boldsymbol{V}}^\kappa(\text{div}_\Gamma \boldsymbol{\mu})(\mathbf{x})$$
$$\boldsymbol{\Psi}_{DL}^\kappa(\boldsymbol{\mu})(\mathbf{x}) := \mathbf{curl}_{\mathbf{x}} \boldsymbol{\Psi}_{\boldsymbol{V}}^\kappa(\boldsymbol{\mu})(\mathbf{x})$$

Now, following, for example, the derivation in [3, section4] it is possible to formulate the famous Stratton-Chu representation formula.

Theorem 3 (Stratton-Chu representation formula)**.** *Any Maxwell solution* $\mathbf{u}$ *in* Ω_s *possesses the representation*

$$\mathbf{u} = \mathbf{\Psi}_{DL}^{\kappa}(\gamma_{\mathbf{t}}^{-}) + \mathbf{\Psi}_{SL}^{\kappa}(\gamma_N^{-}) \quad \text{in } \boldsymbol{H}_{\mathrm{loc}}(\mathbf{curl}^2, \Omega_s).$$

If $\mathbf{u}$ *is a Maxwell solution in* Ω' *that satisfies the Silver-Müller radiation conditions, it can be written as*

$$\mathbf{u} = -\mathbf{\Psi}_{DL}^{\kappa}(\gamma_{\mathbf{t}}^{+}) - \mathbf{\Psi}_{SL}^{\kappa}(\gamma_N^{+}) \quad \text{in } \boldsymbol{H}(\mathbf{curl}^2, \Omega').$$

Where we indicated with the superscripts $^{+/-}$ the traces from the inside and the outside of Γ.

3.2 Boundary Integral Operators

In this section we define the BIOs related to the Maxwell problem and we analyze some of their properties which we will use in order to prove that the augmented EFIE is well-posed.
The classical way of building the BIOs is to compose averaging of traces and layer potentials. In the following, we will use the notation $\{\gamma_*\}_\Gamma = \frac{1}{2}\left(\gamma_*^{+} + \gamma_*^{-}\right)$ to indicate the averaging of any trace γ_* at the interface Γ.
Although in other contexts four BIOs originate, here the relations

$$\begin{aligned}\mathbf{curl} \circ \mathbf{\Psi}_{SL}^{\kappa} &= \kappa \mathbf{\Psi}_{DL},\\ \mathbf{curl} \circ \mathbf{\Psi}_{DL}^{\kappa} &= \kappa \mathbf{\Psi}_{SL},\end{aligned}$$

imply

$$\begin{aligned}\gamma_N^{\pm} \mathbf{\Psi}_{SL}^{\kappa} &= \gamma_{\mathbf{t}}^{\pm} \mathbf{\Psi}_{DL}^{\kappa},\\ \gamma_N^{\pm} \mathbf{\Psi}_{DL}^{\kappa} &= \gamma_{\mathbf{t}}^{\pm} \mathbf{\Psi}_{SL}^{\kappa}.\end{aligned}$$

Then we reduce to have only the two following BIOs:

$$\begin{aligned}\mathbf{S}_\kappa &:= \{\gamma_{\mathbf{t}}\}_\Gamma \circ \mathbf{\Psi}_{SL}^{\kappa} = \{\gamma_N\}_\Gamma \circ \mathbf{\Psi}_{DL}^{\kappa}\\ \mathbf{C}_\kappa &:= \{\gamma_{\mathbf{t}}\}_\Gamma \circ \mathbf{\Psi}_{DL}^{\kappa} = \{\gamma_N\}_\Gamma \circ \mathbf{\Psi}_{SL}^{\kappa}\end{aligned}$$

According to [3, Section 5] we have the continuity of both of the operators.

Corollary 1. *The operators* $\mathbf{S}_\kappa$,$\boldsymbol{S}_\kappa : \boldsymbol{H}_\times^{-\frac{1}{2}}(\mathrm{div}_\Gamma, \Gamma) \to \boldsymbol{H}_\times^{-\frac{1}{2}}(\mathrm{div}_\Gamma, \Gamma)$ *are continuous.*

Following the same procedure we can also define the two single layer BIOs

$$\begin{aligned}V_\kappa &:= \{\gamma\}_\Gamma \circ \Psi_V^{\kappa}\\ \mathbf{V}_\kappa &:= \{\gamma_{\mathbf{t}}\}_\Gamma \circ \mathbf{\Psi}_{\boldsymbol{V}}^{\kappa}\end{aligned}$$

which are also continuous.

Corollary 2. *The operators* $V_\kappa : H^{-\frac{1}{2}}(\Gamma) \to H^{-\frac{1}{2}}(\Gamma)$ *and* $\mathbf{V}_\kappa : \boldsymbol{H}_\times^{-\frac{1}{2}}(\Gamma) \to \boldsymbol{H}_\times^{-\frac{1}{2}}(\Gamma)$ *are continuous.*

Both $\mathbf{S}_\kappa$ and $\mathbf{C}_\kappa$ allow a variational formulation, for two tangential vector fields $\boldsymbol{\mu}, \boldsymbol{\xi} \in \boldsymbol{L}^\infty(\Gamma)$

$$\begin{aligned}
\langle \mathbf{S}_\kappa \boldsymbol{\mu}, \boldsymbol{\xi} \rangle_{\tau,\Gamma} &= -\kappa \int_\Gamma \int_\Gamma E_\kappa(\mathbf{x}-\mathbf{y}) \boldsymbol{\mu}(\mathbf{y}) \cdot \boldsymbol{\xi}(\mathbf{x}) \mathrm{d}S(\mathbf{y},\mathbf{x}) + \\
&+ \frac{1}{\kappa} \int_\Gamma \int_\Gamma E_\kappa(\mathbf{x}-\mathbf{y}) \mathrm{div}_\Gamma \boldsymbol{\mu}(\mathbf{y}) \mathrm{div}_\Gamma \boldsymbol{\xi} \mathrm{d}S(\mathbf{y},\mathbf{x}), \\
\langle \mathbf{C}_\kappa \boldsymbol{\mu}, \boldsymbol{\xi} \rangle_{\tau,\Gamma} &= -\int_\Gamma \int_\Gamma \mathbf{grad}_\mathbf{x} E_\kappa(\mathbf{x}-\mathbf{y}) \cdot (\boldsymbol{\mu}(\mathbf{y}) \times \boldsymbol{\xi}(\mathbf{x})) \mathrm{d}S(\mathbf{y},\mathbf{x}).
\end{aligned}$$

We conclude this section showing some useful properties of the single layer BIOs.

Lemma 1. *The integral operators $\delta V_\kappa = V_\kappa - V_0 : H^{-\frac{1}{2}}(\Gamma) \to H^{\frac{1}{2}}(\Gamma)$ and $\delta \mathbf{V}_\kappa = \mathbf{V}_\kappa - \mathbf{V}_0 : \boldsymbol{H}_\times^{-\frac{1}{2}}(\Gamma) \to \boldsymbol{H}_\times^{\frac{1}{2}}(\Gamma)$ are compact.*

Proof. See proof of Lemma 3.2 in [8] □

Lemma 2. *The operators V_0 and $\mathbf{V}_0$ are continuous, selfadjoint with respect to the bilinear pairings $\langle \cdot, \cdot \rangle_{\frac{1}{2},\Gamma}$ and $\langle \cdot, \cdot \rangle_{\boldsymbol{\tau},\Gamma}$, respectively, and satisfy*

$$\begin{aligned}
\langle \mu, V_0 \bar{\mu} \rangle_{\frac{1}{2},\Gamma} &\geq C \|\mu\|^2_{H^{-\frac{1}{2}}(\Gamma)} && \forall \mu \in H^{-\frac{1}{2}}(\Gamma) \\
\langle \boldsymbol{\mu}, \mathbf{V}_0 \bar{\boldsymbol{\mu}} \rangle_{\boldsymbol{\tau},\Gamma} &\geq C \|\boldsymbol{\mu}\|^2_{\boldsymbol{H}_\times^{-\frac{1}{2}}(\Gamma)} && \forall \mu \in \boldsymbol{H}_\times^{-\frac{1}{2}}(\mathrm{div}_\Gamma 0, \Gamma)
\end{aligned}$$

with constants $C > 0$ depending on Γ.

Proof. A proof can be found, for example, in Theorem 6.2 of [7]. □

The typical strategy now would be to derive some jump relations and then use them together with the definition of BIOs by averaging of traces and the representation formula. This approach results in the so called direct BIEs. An extended explanation of how to derive the direct BIE for the electromagnetic scattering can be found in [3]. In the following we will proceed differently and we will find an indirect BIE.

3.3 Boundary Integral Equations

As usual in BEM, we can formulate different kinds of BIE. Here we focus on the indirect approach. First, we define $\mathbf{E}^t = \mathbf{E}_s + \mathbf{E}_{inc}$, where $\mathbf{E}_{inc}$ is the incident field and $\mathbf{E}_s$ is the scattered field. Then we call $\boldsymbol{j}^t$ the jump of the Neumann trace of $\mathbf{E}^t$, that is the surface current on Γ,

$$\boldsymbol{j}^t = \left[\gamma_N \mathbf{E}^t\right]_\Gamma = \gamma_N(\mathbf{E}^t_{|\Omega'}) - \gamma_N(\mathbf{E}^t_{|\Omega_s}).$$

Since we will work with a scatterer which is a Perfectly Electric Conductor, we can now impose $\mathbf{E}_{|\Omega_s} = 0$ and we simply write

$$\boldsymbol{j}^t = \gamma_N(\mathbf{E}^t_{|\Omega'}).$$

The idea, now, is to impose a representation of the electric field of the form

$$\mathbf{E}_s = -\boldsymbol{\Psi}_{SL}(\boldsymbol{j}^t) \quad \text{in } \boldsymbol{H}_{\mathrm{loc}}(\mathbf{curl}^2, \Omega_s \cup \Omega'),$$

If we apply the exterior Dirichlet trace $\gamma_{\mathbf{t}}^+$ to $\mathbf{E}_s$, keeping in mind the boundary condition $\gamma_{\mathbf{t}}^+\mathbf{E}_s = -\gamma_{\mathbf{t}}^+\mathbf{E}_i$, we get the Boundary Integral Equation

$$\mathbf{S}_\kappa \boldsymbol{j}^t = -\gamma_{\mathbf{t}}^+\mathbf{E}_i \quad \text{in } \boldsymbol{H}_\times^{-\frac{1}{2}}(\mathrm{div}_\Gamma, \Gamma),$$

which can be cast in the following variational weak form: find $\boldsymbol{j}^t \in \boldsymbol{H}_\times^{-\frac{1}{2}}(\mathrm{div}_\Gamma, \Gamma)$ such that

$$\langle \mathbf{S}_\kappa \boldsymbol{j}^t, \boldsymbol{\mu}\rangle_{\boldsymbol{\tau},\Gamma} = -\langle \gamma_{\mathbf{t}}^+\mathbf{E}_i, \boldsymbol{\mu}\rangle_{\boldsymbol{\tau},\Gamma} \quad \forall \boldsymbol{\mu} \in \boldsymbol{H}_\times^{-\frac{1}{2}}(\mathrm{div}_\Gamma, \Gamma).$$

This equation and its boundary element discretization can be proved to be well-posed when κ^2 is not an interior electric eigenvalue as it has been done in [3]. Unfortunately this formulation encounters problems when $\kappa \to 0$ due to the $\frac{1}{\kappa}$ term in

$$\langle \mathbf{S}_k \boldsymbol{j}^t, \boldsymbol{\mu}\rangle_{\boldsymbol{\tau},\Gamma} = -\kappa \langle V_\kappa \mathrm{div}_\Gamma \boldsymbol{j}^t, \mathrm{div}_\Gamma \boldsymbol{\mu}\rangle_{\frac{1}{2},\Gamma} + \frac{1}{\kappa}\langle \mathbf{V}_\kappa \boldsymbol{j}^t, \boldsymbol{\mu}\rangle_{\frac{1}{2},\Gamma}.$$

In order to overcome this instability, an augmented formulation as been introduced which is proved to be stable also for small κ. For the details one can see for example [11]. The main idea is to introduce the surface charge ρ_Γ^t and explicitly impose in the formulation the continuity equation in weak form

$$\langle V_\kappa \mathrm{div}_\Gamma \boldsymbol{j}^t, v\rangle_{\frac{1}{2},\Gamma} = -\kappa^2 \langle V_\kappa \rho_\Gamma^t, v\rangle_{\frac{1}{2},\Gamma} \quad \forall v \in H(\Gamma)^{-\frac{1}{2}},$$

The obtained augmented variational formulation is: find $(\boldsymbol{j}^t, \rho_\Gamma^t) \in \boldsymbol{H}_\times^{-\frac{1}{2}}(\mathrm{div}_\Gamma, \Gamma) \times H^{-\frac{1}{2}}(\Gamma)$ such that for any $(\boldsymbol{\mu}, v) \in \boldsymbol{H}_\times^{-\frac{1}{2}}(\mathrm{div}_\Gamma, \Gamma) \times H^{-\frac{1}{2}}(\Gamma)$

$$\begin{cases} \langle \mathbf{V}_\kappa \boldsymbol{j}^t, \boldsymbol{\mu}\rangle_{\frac{1}{2},\Gamma} + \langle V_\kappa \rho_\Gamma^t, \mathrm{div}_\Gamma \boldsymbol{\mu}\rangle_{\frac{1}{2},\Gamma} & = -\langle \gamma_{\mathbf{t}} \mathbf{e}_i, \boldsymbol{\mu}\rangle_{\boldsymbol{\tau},\Gamma}, \\ \langle V_\kappa \mathrm{div}_\Gamma \boldsymbol{j}^t, v\rangle_{\frac{1}{2},\Gamma} + \kappa^2 \langle V_\kappa \rho_\Gamma^t, v\rangle_{\frac{1}{2},\Gamma} & = 0, \end{cases} \tag{1}$$

4 Discretization

In this section we aim at discretizing problem 1 so that it can be rewritten as a linear system. In order to obtain the discretized problem, we need to define the boundary element spaces which will substitute the spaces $\boldsymbol{H}_{\times}^{-\frac{1}{2}}(\mathrm{div}_\Gamma, \Gamma)$ and $H^{-\frac{1}{2}}(\Gamma)$. After having defined the discrete spaces, it will be easy to apply a Galerkin discretization to our system.

4.1 Boundary Element Spaces

First, we introduce a triangular mesh Γ_h on the piecewise smooth surface Γ with a perfect resolution, that is $\Gamma = \bar{K_1} \cup \cdots \cup \bar{K_N}$ where $\mathcal{K} = \{K_1, ..., K_N\}$ is the set of the cells of the triangulation. Furthermore, we assume that no cell straddles the edges of Γ. Now we can define a diffeormorphism $\boldsymbol{\Phi}_k : \hat{K} \to \bar{K}$ from the unit triangle to any cell K which allows us to define the boundary element spaces on the reference triangle and lift them to the triangulation via pull-back. To discretize $\boldsymbol{H}_{\times}^{-\frac{1}{2}}(\mathrm{div}_\Gamma, \Gamma)$ we will use the zeroth order triangular Raviart-Thomas element space, defined as (see [3]):

Definition 5. *For $\kappa \in \mathbb{N}_0$, we define the k-th order Raviart-Thomas boundary element space by*

$$\mathcal{RT}^k_{\mathcal{K}} = \{\boldsymbol{\mu} \in \boldsymbol{H}_{\times}^{-\frac{1}{2}}(\mathrm{div}_\Gamma, \Gamma), \boldsymbol{\mu}_{|K} \in \mathfrak{F}_K(\mathcal{RT}^k(\hat{K})), \forall K \in \mathcal{K}\}$$

where $\mathfrak{F}_K$ is the Piola transform

$$(\mathfrak{F}_K \boldsymbol{\mu})(\mathbf{x}) = \sqrt{\mathrm{detG}}\mathrm{G}^{-1} D\boldsymbol{\Phi}_K^T(\hat{\mathbf{x}})\boldsymbol{\mu}(\hat{\mathbf{x}}),$$
$$\mathrm{G} = D\boldsymbol{\Phi}_K^T(\hat{\mathbf{x}})D\boldsymbol{\Phi}_K(\hat{\mathbf{x}}), \quad \mathbf{x} = \boldsymbol{\Phi}(\hat{\mathbf{x}}),\ \mathbf{x} \in K,$$

and

$$\begin{aligned}\mathcal{RT}^k(\hat{K}) :&= (\mathcal{P}_k(\hat{K}))^2 \oplus (\hat{\mathbf{x}}\tilde{\mathcal{P}}_k(\hat{K})) \\ &= \{\hat{\mathbf{x}} \to \mathbf{p}(\hat{\mathbf{x}}) + q(\hat{\mathbf{x}})\hat{\mathbf{x}},\ \hat{\mathbf{x}} \in \hat{K},\ \mathbf{p} \in (\mathcal{P}_k(\hat{K}))^2,\ q \in \tilde{\mathcal{P}}_k(\hat{K})\},\end{aligned}$$

and $\mathcal{P}_k(\hat{K})$ contains all the multivariate polynomials of total degree $k \in \mathbb{N}_0$ on $\hat{K}$ and $\tilde{\mathcal{P}}_k(\hat{K})$ represents all the homogeneous multivariate polynomials of degree $k \in \mathbb{N}_0$.

In the following we indicate $\mathcal{Q} = {\mathcal{RT}_{\mathcal{K}}}^0$. Moreover, keeping in mind Theorem 2, we discretize the space $\boldsymbol{H}_{\perp}^{-\frac{1}{2}}(\mathbf{curl}_\Gamma, \Gamma)$ by a rotated version of $\mathcal{Q}$, which we call $\mathcal{E} = \mathbf{R}\mathcal{Q}$. On the other hand, we discretize $H_{\times}^{-\frac{1}{2}}(\Gamma)$ using the space spanned by the Lagrangian piecewise constant basis functions, $\mathcal{V}$.

In the rest of the section we will use the following notations for the global basis functions:

Boundary Element Space	Global Basis Function
$\mathcal{Q}$	$\boldsymbol{\phi}_i$
$\mathcal{E}$	$\boldsymbol{\phi}^i$
$\mathcal{V}$	β_i

On the reference triangle $\hat{T} = \{(\hat{x}_1, \hat{x}_2) | 0 < \hat{x}_2 < \hat{x}_1 < 1\}$, the local basis functions of $\mathcal{RT}^0_{\mathcal{K}}$ are:

$$\hat{\boldsymbol{\phi}}_{12} = \begin{bmatrix} \hat{x}_1 - 1 \\ \hat{x}_2 - 1 \end{bmatrix} \quad \hat{\boldsymbol{\phi}}_{23} = \begin{bmatrix} \hat{x}_1 \\ \hat{x}_2 \end{bmatrix} \quad \hat{\boldsymbol{\phi}}_{31} = \begin{bmatrix} \hat{x}_1 - 1 \\ \hat{x}_2 \end{bmatrix}.$$

The subscripts ij indicate that the function is associated with the edge joining the nodes i and j.

4.2 Discretization of the EFIE

We use the previously defined Boundary Element Spaces to build the linear systems corresponding to the two formulations of the EFIE. We can define the discretized functions:

$$\boldsymbol{j}^t_N = \sum_{i=1}^{N_{\mathcal{Q}}} m_i \boldsymbol{\phi}_i, \qquad -\gamma_{\mathbf{t}} \mathbf{E}_{i\,N} = \sum_{i=1}^{N_{\mathcal{Q}}} \mu_i \boldsymbol{\phi}_i.$$

Exploiting the bilinearity of the forms $\langle \mathbf{V}_\kappa \cdot, \cdot \rangle_{\frac{1}{2},\Gamma}$, $\langle V_\kappa \cdot, \cdot \rangle_{\frac{1}{2},\Gamma}$ and $\langle \cdot, \cdot \rangle_{\tau,\Gamma}$ and the linearity of div_Γ, we obtain the discretized version of the EFIE

$$\sum_{i=1}^{N_{\mathcal{Q}}} m_i \langle \mathbf{V}_\kappa \boldsymbol{\phi}_i, \boldsymbol{\phi}_j \rangle_{\frac{1}{2},\Gamma} - \frac{1}{\kappa^2} \sum_{i=1}^{N_{PW}} \psi_i \langle V_\kappa \mathrm{div}_\Gamma \boldsymbol{\phi}_i, \mathrm{div}_\Gamma \boldsymbol{\phi}_j \rangle_{\frac{1}{2},\Gamma} = \sum_{i=1}^{N_{\mathcal{Q}}} \mu_i \langle \boldsymbol{\phi}_i, \boldsymbol{\phi}_j \rangle_{\tau,\Gamma},$$

It is useful to introduce the following matrices and vectors

$$\begin{aligned}
&[\mathbf{A}]_{i,j} = \langle \mathbf{V}_\kappa \boldsymbol{\phi}_i, \boldsymbol{\phi}_j \rangle_{\frac{1}{2},\Gamma} \in \mathbb{R}^{N_{\mathcal{Q}} \times N_{\mathcal{Q}}}, \\
&[\tilde{\mathbf{V}}]_{i,j} = \langle \mathbf{V}_\kappa \mathrm{div}_\Gamma \boldsymbol{\phi}_i, \mathrm{div}_\Gamma \boldsymbol{\phi}_j \rangle_{\frac{1}{2},\Gamma} \in \mathbb{R}^{N_{\mathcal{Q}} \times N_{\mathcal{Q}}}, \\
&[\mathbf{M}]_{i,j} = \langle \boldsymbol{\phi}_i, \boldsymbol{\phi}_j \rangle_{\tau,\Gamma} \in \mathbb{R}^{N_{\mathcal{Q}} \times N_{\mathcal{Q}}}, \\
&[\mathbf{m}]_i = m_i \in \mathbb{R}^{N_{\mathcal{Q}}}, \\
&[\boldsymbol{\mu}]_i = \mu_i \in \mathbb{R}^{N_{\mathcal{Q}}}.
\end{aligned}$$

To assemble the mass matrix we use $\boldsymbol{\phi}^i = \boldsymbol{\phi}_i \times \mathbf{n}$ and we get

$$[\mathbf{M}]_{i,j} = \langle \boldsymbol{\phi}_i, \boldsymbol{\phi}_j \rangle_{\tau,\Gamma} = \langle \boldsymbol{\phi}_i \times \mathbf{n}, \boldsymbol{\phi}_j \rangle_{\frac{1}{2},\Gamma} = \langle \boldsymbol{\phi}^i, \boldsymbol{\phi}_j \rangle_{\frac{1}{2},\Gamma}.$$

Therefore, the discretized EFIE becomes

$$\left(\mathbf{A} - \frac{1}{k^2} \tilde{\mathbf{V}} \right) \mathbf{m} = \mathbf{M} \boldsymbol{\mu}$$

4.3 Discretization of the Stabilized Formulation

For the stabilized formulation we need to introduce the discretized version of ρ_N^t

$$\rho_N^t = \sum_{i=1}^{N_\mathcal{V}} \psi_i \beta_i.$$

Then by the same arguments used in the previous subsection we can rewrite (1) as

$$\begin{cases} \sum_{i=1}^{N_\mathcal{Q}} m_i \langle \mathbf{V}_\kappa \boldsymbol{\phi}_i, \boldsymbol{\phi}_j \rangle_{\frac{1}{2},\Gamma} + \sum_{i=1}^{N_{PW}} \psi_i \langle V_\kappa \beta_i, \mathrm{div}_\Gamma \boldsymbol{\phi}_j \rangle_{\frac{1}{2},\Gamma} & = \sum_{i=1}^{N_\mathcal{Q}} \mu_i \langle \boldsymbol{\phi}_i, \boldsymbol{\phi}_j \rangle_{\tau,\Gamma}, \\ \sum_{i=1}^{N_\mathcal{Q}} m_i \langle V_\kappa \mathrm{div}_\Gamma \boldsymbol{\phi}_i, \beta_j \rangle_{\frac{1}{2},\Gamma} - \kappa^2 \sum_{i=1}^{N_\mathcal{Q}} \psi_i \langle V_\kappa \beta_i, \beta_j \rangle_{\frac{1}{2},\Gamma} & = 0. \end{cases}$$

If we now write

$$\begin{aligned} [\mathbf{V}]_{i,j} &= \langle V_\kappa \beta_i, \beta_j \rangle_{\frac{1}{2},\Gamma} \in \mathbb{R}^{N_\mathcal{V} \times N_\mathcal{V}}, \\ [\mathbf{Q}]_{i,j} &= \langle V_\kappa \beta_i, \mathrm{div}_\Gamma \boldsymbol{\phi}_j \rangle_{\frac{1}{2},\Gamma} \in \mathbb{R}^{N_\mathcal{V} \times N_\mathcal{V}}, \\ [\boldsymbol{\psi}]_i &= \psi_i \in \mathbb{R}^{N_\mathcal{V}}, \end{aligned}$$

the discretized version can be compactly rewritten as

$$\begin{bmatrix} \mathbf{A} & \mathbf{Q} \\ \mathbf{Q}^T & \kappa^2 \mathbf{V} \end{bmatrix} \begin{bmatrix} \mathbf{m} \\ \boldsymbol{\psi} \end{bmatrix} = \begin{bmatrix} \mathbf{M}\boldsymbol{\mu} \\ \mathbf{0}_{N_\mathcal{V} \times 1} \end{bmatrix}.$$

4.4 The Divergence Matrix

In this subsection we characterize the matrices $\tilde{\mathbf{V}}$ and $\mathbf{Q}$, in order to simplify their implementation, by showing that they can be written as products of simpler matrices. All the ideas here presented are extensively discussed in [10].
First of all, we show that in our Boundary Element Spaces div_Γ can be replaced by a matrix $\mathbf{D}$. To see this it is useful to recall that the surface divergence is a linear and surjective transformation as a mapping

$$\mathrm{div}_\Gamma : \mathcal{Q} \longrightarrow \mathcal{V}^*.$$

where $\mathcal{V}^*$ is space of the functions in $\mathcal{V}$ with zero mean. This is shown, for example, in Lemma 5.4 of [1]. Then for any basis function of $\mathcal{Q}$ we can write:

$$\mathrm{div}_\Gamma \boldsymbol{\phi}_i = \sum_{j=1}^{N_\mathcal{V}} d_{ij} \beta_j,$$

and, thus, we can associate the matrix $[\mathbf{D}]_{ij} = d_{ij} \in \mathbb{R}^{N_\mathcal{Q} \times N_\mathcal{V}}$ to the surface divergence. Now it is easy to derive the factorizations of $\tilde{\mathbf{V}}$ and $\mathbf{Q}$. First, we have

$$[\mathbf{Q}]_{ij} = \langle V_\kappa \beta_i, \mathrm{div}_\Gamma \boldsymbol{\phi}_j \rangle_{\frac{1}{2},\Gamma} = \langle V_\kappa \beta_i, \sum_{i=1}^{N_\mathcal{V}} d_{jl} \beta_l \rangle_{\frac{1}{2},\Gamma} = \sum_{i=1}^{N_\mathcal{V}} d_{jl} \langle V_\kappa \beta_i, \beta_l \rangle_{\frac{1}{2},\Gamma},$$

which means $\mathbf{Q} = \mathbf{D}\mathbf{V}^T$.
Moreover,

$$[\tilde{\mathbf{V}}]_{ij} = \langle V_\kappa \mathrm{div}_\Gamma \boldsymbol{\phi}_i, \mathrm{div}_\Gamma \boldsymbol{\phi}_j \rangle_{\frac{1}{2},\Gamma} = \langle V_\kappa \sum_{l=1}^{N_\mathcal{V}} d_{il}\beta_l, \sum_{t=1}^{N_\mathcal{V}} d_{jt}\beta_t \rangle_{\frac{1}{2},\Gamma} =$$
$$= \sum_{l=1}^{N_\mathcal{V}} d_{il} \sum_{t=1}^{N_\mathcal{V}} d_{jt} \langle V_\kappa \beta_l, \beta_t \rangle_{\frac{1}{2},\Gamma} = \sum_{l=1}^{N_\mathcal{V}} d_{il} [\mathbf{V}]_{jl}$$

,

that is

$$[\tilde{\mathbf{V}}] = \mathbf{D}\mathbf{Q}^T = \mathbf{D}\mathbf{V}\mathbf{D}^T.$$

5 Well-Posedness of Augmented EFIE (Continuous and Discrete)

In this section we aim at proving existence and uniqueness of the saddle point problem (1) both in continuous and discrete form. First, we report some general results from [1] and then we show that (1) satisfies the necessary and sufficient conditions for well-posedness.

5.1 Saddle Point Problems

In this subsection we use the same notation as [1], thus every symbol should be read independently from its meaning in the other sections.
We start by defining a saddle point problem with penalty term.

Definition 6. *Suppose that X and M are two Hilbert spaces, given a bilinear form $a(\cdot,\cdot) : X \times X \to \mathbb{R}$ such that $a(v,v) \geq 0 \quad \forall v \in X$ and a bilinear form $b(\cdot,\cdot) : X \times M \to \mathbb{R}$, the problem to find $(u,\lambda) \in X, M$ such that*

$$\begin{aligned} a(u,v)+b(v,\lambda) &= \langle f, v\rangle \quad \forall v \in X, \\ b(u,\mu) \qquad\quad &= \langle g, \mu\rangle \quad \forall \mu \in M, \end{aligned}$$

is a saddle point problem.

The saddle point problem defines a mapping

$$\begin{aligned} L &: X \times M \longrightarrow X' \times M' \\ L &: (u,\lambda) \longmapsto (f,g) \end{aligned}$$

Therefore, we need to show that L is an isomorphism in order two prove that the inverse mapping L^{-1} associates to every (f,g) couple one and only one (u,λ) couple. In order to do this it is useful to define the space

$$V := \{v \in X : b(v,\mu) = 0 \quad \forall \mu \in M\}$$

Now we are ready to report the main result about saddle point problems from [1].

Theorem 4. *For a saddle point problem the mapping L defines an isomorphism if and only if the following conditions are satisfied:*

1. *a is V-elliptic, i.e.*

$$\big|a(v,v)\big| \geq \alpha \|v\|_V^2 \quad \forall v \in V,$$

   where $\alpha > 0$

2. *The bilinear form b satisfies the inf-sup condition;*

$$\sup_{v \in X} \frac{b(v,\mu)}{\|v\|_X} \geq \beta \|\mu\|_M \quad \forall \mu \in M,$$

   with $\beta > 0$;

5.2 Inf-sup Conditions

Using the abstract results from the previous section we can prove the well-posedness of problem (1).
First it is important to recall that the BIOs V_κ and $\mathbf{V}_\kappa$ can be obtained by adding a compact perturbation to V_0 and $\mathbf{V}_0$ (see lemma 1). Now we consider the problem to find $(\boldsymbol{j}^t, \rho_\Gamma^t) \in \boldsymbol{H}_\times^{-\frac{1}{2}}(\mathrm{div}_\Gamma, \Gamma) \times H^{-\frac{1}{2}}(\Gamma)$ such that for any $(\boldsymbol{\mu}, v) \in \boldsymbol{H}_\times^{-\frac{1}{2}}(\mathrm{div}_\Gamma, \Gamma) \times H^{-\frac{1}{2}}(\Gamma)$

$$\begin{cases} \langle \mathbf{V}_0 \boldsymbol{j}^t, \boldsymbol{\mu} \rangle_{\frac{1}{2},\Gamma} + \langle V_0 \rho_\Gamma^t, \mathrm{div}_\Gamma \boldsymbol{\mu} \rangle_{\frac{1}{2},\Gamma} & = \langle \gamma_{\mathbf{t}} \mathbf{e}_i, \boldsymbol{\mu} \rangle_{\frac{1}{2},\Gamma}, \\ \langle V_0 \mathrm{div}_\Gamma \boldsymbol{j}^t, v \rangle_{\frac{1}{2},\Gamma} & = 0. \end{cases} \tag{2}$$

Problem 1 and 2 respectively define the two operators L_κ and L_0. Given lemma 1, it can also be shown, as it has been done in section 5.2 of [4], that the operator $\delta L_\kappa = L_\kappa - L_0$ is compact. This point is really important because, having the compactness of δL_κ, if we prove that L_0 is an isomorphism then also L_k will be, by Fredholm's Alternative, if it is injective. Thus, we can focus on problem 2 and use Theorem 4 to prove that L_0 is an isomorphism.
An important step is to observe that the equation $\langle V_0 \mathrm{div}_\Gamma \boldsymbol{j}^t, v \rangle_{\frac{1}{2},\Gamma} = 0 \ \forall v \in H^{-\frac{1}{2}}(\Gamma)$ implies $\mathrm{div}_\Gamma \boldsymbol{j}^t = 0$ in $H^{-\frac{1}{2}}(\Gamma)$ and, therefore, it is sufficient to consider $\boldsymbol{j}^t \in \boldsymbol{H}^{-\frac{1}{2}}(\mathrm{div}_\Gamma 0, \Gamma)$. Lemma 2 gives the coercivity of $\mathbf{V}_\kappa$ in $\boldsymbol{H}^{-\frac{1}{2}}(\mathrm{div}_\Gamma 0, \Gamma)$ and of V_κ in $H^{-\frac{1}{2}}(\Gamma)$. Therefore, by theorem 4, if the bilinear form $\langle V_0 \rho, \mathrm{div}_\Gamma \boldsymbol{\iota} \rangle_{\frac{1}{2},\Gamma}$ satisfies the inf-sup condition L_0 is an isomorphism. The following theorem, which has been proved in [10], gives us the desired inf-sup condition.

Theorem 5. *There exists a constant $C \geq 0$ such that*

$$\sup_{0 \neq \boldsymbol{\phi} \in H^{-\frac{1}{2}}(\mathrm{div}_\Gamma, \Gamma)} \frac{\langle V_\kappa \mathrm{div}_\Gamma \boldsymbol{\phi}, v \rangle_{\frac{1}{2},\Gamma}}{\|\boldsymbol{\phi}\|_{\boldsymbol{H}^{-\frac{1}{2}}(\mathrm{div}_\Gamma, \Gamma)}} \geq C \|v\|_{H^{-\frac{1}{2}}(\Gamma)}$$

holds for all $v \in H_{**}^{-\frac{1}{2}}(\Gamma) = \{u \in H^{-\frac{1}{2}} : \langle u, V_\kappa 1 \rangle = 0\}$.

Moreover, it is necessary to prove that problem 1 is also well-posed when using the discrete spaces $\mathcal{Q}$ and $\mathcal{V}$. This can be easily shown using the same reasoning as before, which makes it necessary to find a discrete inf-sup condition. The rigorous derivation can be found in [6], we again only report the main result.

Theorem 6. *There exists a constant $C \geq 0$ such that*

$$\sup_{0 \neq \boldsymbol{\phi}_h \in \mathcal{Q}} \frac{\langle V_\kappa \mathrm{div}_\Gamma \boldsymbol{\phi}_h, v_h \rangle_{\frac{1}{2},\Gamma}}{\|\boldsymbol{\phi}_h\|_{\boldsymbol{H}^{-\frac{1}{2}}(\mathrm{div}_\Gamma, \Gamma)}} \geq C \|v_h\|_{H^{-\frac{1}{2}}(\Gamma)}$$

holds for all $v_h \in \mathcal{V}$.

Therefore, also the discretized version of 1 is well-posed.

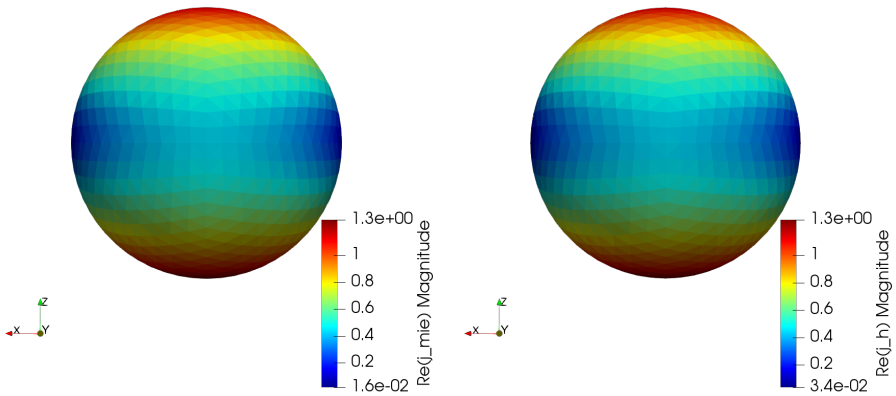

Fig. 1: Comparison of the real part of the Mie Solution (left) and the real part of the numerical solution (right).

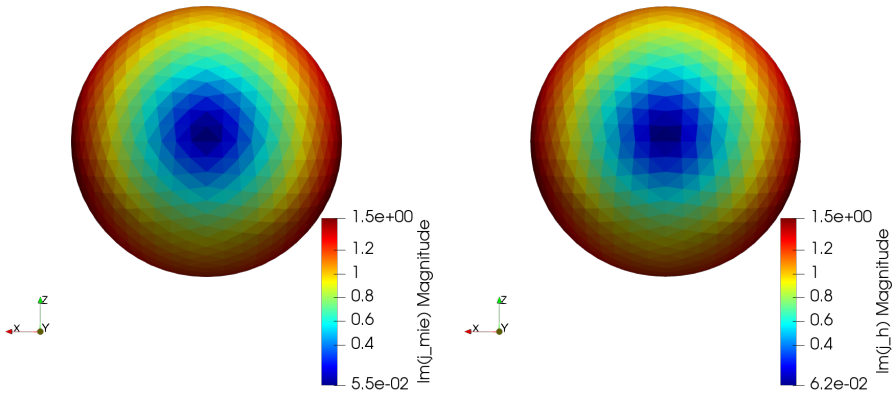

Fig. 2: Comparison of the imaginary part of the Mie Solution (left) and the imaginary part of the numerical solution (right) with 2048 elements and $\kappa = 1$.

6 Numerical Results

In this section we show the results of the C++ implementations based on the BETL2 library [9] of the two versions of the EFIE. We considered the two test cases of a sphere and a cube hit by a plane wave.

6.1 Scattering by a Sphere

The case of a sphere hit by a plane wave is called Mie Scattering and the analytical solution is known (it can be found in the appendix), thus we can compare the numerical solution to the theoretical one, in order to validate of the code. The following tables report the refinement results obtained running the standard version of the EFIE for decreasing values of κ.

Elements	$\|\boldsymbol{\jmath}_h^t - \boldsymbol{\jmath}_{mie}^t\|_2$	$\|\boldsymbol{\jmath}_h^t\|_2$	$\|\boldsymbol{\jmath}_{mie}^t\|_2$	$\frac{\|\boldsymbol{\jmath}_h^t - \boldsymbol{\jmath}_{mie}^t\|_2}{\|\boldsymbol{\jmath}_{mie}^t\|_2}$	Order
$\kappa = 1$					
32	6.590e-1	2.057	2.373	2.776e-1	/
128	2.597e-1	2.257	2.333	1.112e-1	1.3433
512	1.215e-1	2.312	2.331	5.212e-2	1.0956
$\kappa = 0.01$					
32	2.065e-3	1.535e-4	2.212e-3	9.337e-1	/
128	1.980e-3	1.972e-4	2.173e-3	9.337e-1	0.0606
512	1.966e-3	2.094e-4	2.170e-3	9.057e-1	0.0105
$\kappa = 0.0001$					
32	2.065e-5	1.535e-6	2.122 e-5	9.337e-1	/
128	1.980e-5	1.972e-6	2.173e-5	9.114e-1	0.0607
512	1.966e-5	2.094e-6	2.170e-5	9.057e-1	0.0105

As expected we have first order convergence for $\kappa = 1$, but convergence is lost when using a small κ. Fortunately, when using the stabilized version, first order convergence is recovered also for $\kappa \to 0$. The following table shows the results, when the same numerical experiments are carried out using the augmented version.

Elements	$\|\boldsymbol{\jmath}_h^t - \boldsymbol{\jmath}_{mie}^t\|_2$	$\|\boldsymbol{\jmath}_h^t\|_2$	$\|\boldsymbol{\jmath}_{mie}^t\|_2$	$\frac{\|\boldsymbol{\jmath}_h^t - \boldsymbol{\jmath}_{mie}^t\|_2}{\|\boldsymbol{\jmath}_{mie}^t\|_2}$	Order
$\kappa = 1$					
32	6.590e-1	2.057	2.373	2.776e-1	/
128	2.597e-1	2.257	2.333	1.112e-1	1.3433
512	1.215e-1	2.312	2.331	5.212e-2	1.0732
$\kappa = 0.001$					
32	5.837e-4	1.973e-3	2.212e-3	2.638e-1	/
128	2.382e-4	2.118e-3	2.173e-3	1.096e-1	1.2930
512	1.140e-4	2.157e-3	2.170e-3	5.254e-2	1.0621
$\kappa = 0.00001$					
32	5.846e-6	1.973e-5	2.122e-5	2.642e-1	/
128	2.433e-6	2.119e-5	2.119e-5	1.119e-1	1.2647
512	2.073e-6	2.164e-5	2.170e-5	9.550e-2	0.2309

Furthermore, it is also interesting to check that the stabilized formulation is not effected by instabilities when $\kappa \to 0$, differently from the classical version. This can be seen by checking the condition number of the system matrices

$$\mathbf{A}_c = \mathbf{A} - \frac{1}{\kappa^2}\tilde{\mathbf{V}} \qquad \mathbf{A}_s = \begin{bmatrix} \mathbf{A} & \mathbf{Q} \\ \mathbf{Q}^T & \kappa^2\mathbf{V} \end{bmatrix},$$

defined as

$$\mathrm{cond}(\mathbf{A}) = \frac{\max_i |\sigma_i|}{\min_i |\sigma_i|},$$

where σ_i are the eigenvalues of $\mathbf{A}$.
As shown in figure 3, the condition number explodes for the classical formulation, while it does not for the stabilized version, hence the low-frequency instability has been effectively solved.

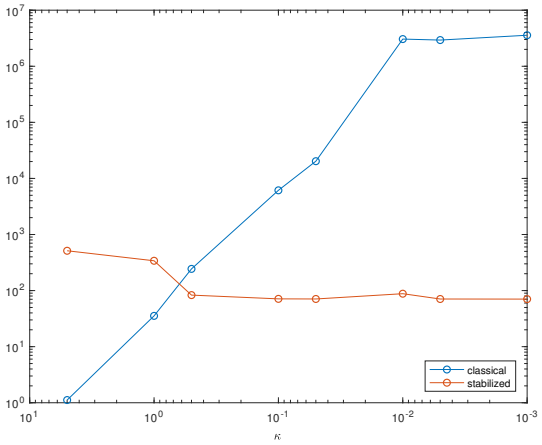

Fig. 3: Condition number of the two formulations for decreasing values of the wavenumber κ on a 128 elements mesh.

Moreover, it is interesting to observe the behavior of the condition number when the mesh is refined. The following table shows the condition number of $\mathbf{A}_c$ for different wavenumbers and refining the mesh.

	32	128	512
$\kappa = 1$	2.034e+1	3.541e+1	7.352e+2
$\kappa = 0.001$	1.896e+6	3.139e+6	1.602e+6
$\kappa = 0.00001$	2.487e+6	2.010e+6	5.994e+6

On the other hand, the following table shows the results for the condition number of $\mathbf{A}_s$

	32	128	512
$\kappa = 1$	4.159e+1	3.401e+1	2.152e+3
$\kappa = 0.001$	2.112e+1	7.050e+1	3.528e+2
$\kappa = 0.00001$	2.112e+1	7.050e+1	3.528e+2

We see that the condition number increases when we refine the mesh. This behavior can cause numerical issues when refining even more the mesh, therefore it should be compensated using some effective preconditioner.

6.2 Scattering by a cube

We also test the code on a cube with unitary length edges. The numerical solution can be qualitatively observed in figure 4. In this case there is no numerical solution available, therefore we compute the difference of the L2 norms of the solutions computed on two consecutive meshes. The results can be found in the following table.

Elements	$\|\boldsymbol{j}_h^t\|_2$	$\|\|\boldsymbol{j}_h^t\|_2 - \|\boldsymbol{j}_{\frac{h}{2}}^t\|_2\|$
$\kappa = 1$		
24	3.265	/
96	3.446	1.810e-1
384	3.534	8.760e-2
$\kappa = 0.001$		
24	2.880e-3	/
96	2.913e-3	3.356e-5
384	2.956e-3	4.200e-5
$\kappa = 0.001$		
24	2.881e-5	/
96	2.914e-5	3.275e-7
384	2.962e-5	4.797e-7

In this case we see that the norm update does not seem to decrease with mesh refinement. We can infer that, given the low number of elements used for these simulations, we are not in asymptotic regime yet, except for the $\kappa = 1$ case, therefore we don't observe the expected convergence.

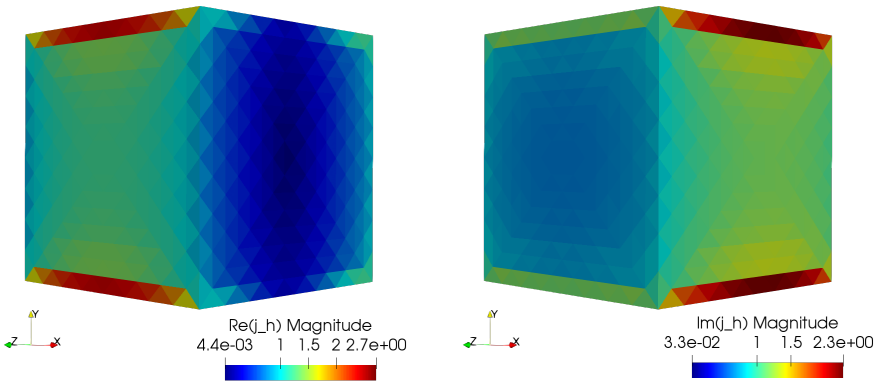

Fig. 4: Numerical solution for the surface current on a unitary cube. The computation has been performed using the standard EFIE with $\kappa = 1$ and a 1536 elements. mesh

7 Conclusions

The numerical results show that we correctly implemented both of the versions of the EFIE. Unfortunately, as it was expected, the convergence is only of first order. To increase the order it would be sufficient to use higher order finite element spaces. On the other hand, our simple implementation is really stable for low frequencies, while the increase in stability does not cause an increase in the error. A noticeable issue is that with the augmented formulation the dimensions of the linear system double. Given that the system matrix is dense, the computational cost of the simulations then becomes considerably higher. Indeed, the increase in the condition number with mesh refinement, which we have observed in subsection 6.1, contributes to making the solution of the system even more burdensome.
One more thing to consider is that we used an indirect formulation, therefore, if the goal was to compute the electric field in the space, we would have to apply the Maxwell Single Layer potential to $\boldsymbol{j}^t$. This can be easily done in BETL, using the single layer potential matrices.

References

[1] Dietrich Braess. *Finite elements*. Third. Theory, fast solvers, and applications in elasticity theory, Translated from the German by Larry L. Schumaker. Cambridge University Press, Cambridge, 2007, pp. xviii+365. ISBN: 978-0-521-70518-9; 0-521-70518-5. DOI: 10.1017/CBO9780511618635. URL: https://doi.org/10.1017/CBO9780511618635.

[2] A. Buffa, M. Costabel, and D. Sheen. "On traces for $\mathbf{H}(\mathbf{curl}, \Omega)$ in Lipschitz domains". In: *J. Math. Anal. Appl.* 276.2 (2002), pp. 845–867. ISSN: 0022-247X. DOI: 10.1016/S0022-247X(02)00455-9. URL: https://doi.org/10.1016/S0022-247X(02)00455-9.

[3] Annalisa Buffa and Ralf Hiptmair. "Galerkin boundary element methods for electromagnetic scattering". In: *Topics in computational wave propagation*. Vol. 31. Lect. Notes Comput. Sci. Eng. Springer, Berlin, 2003, pp. 83–124. DOI: 10.1007/978-3-642-55483-4_3. URL: https://doi.org/10.1007/978-3-642-55483-4_3.

[4] M. Costabel, M. Dauge, and S. Nicaise. *Boundary Value Problems and Integral Equations in Nonsmooth Domains*. Lecture Notes in Pure and Applied Mathematics. Taylor & Francis, 1994. ISBN: 9780824793203. URL: https://books.google.ch/books?id=uZjYdk4bQgkC.

[5] Martin Costabel and Ernst P. Stephan. "Strongly elliptic boundary integral equations for electromagnetic transmission problems". In: *Proc. Roy. Soc. Edinburgh Sect. A* 109.3-4 (1988), pp. 271–296. ISSN: 0308-2105. DOI: 10.1017/S0308210500027773. URL: https://doi.org/10.1017/S0308210500027773.

[6] Sarah Engleder. "Boundary element methods for eddy current transmission problems". Technische Universität Graz, 2011. URL: https://diglib.tugraz.at/download.php?id=576a7b530d312&location=browse.

[7] R. Hiptmair. "Symmetric coupling for eddy current problems". In: *SIAM J. Numer. Anal.* 40.1 (2002), pp. 41–65. ISSN: 0036-1429. DOI: 10.1137/S0036142900380467. URL: https://doi.org/10.1137/S0036142900380467.

[8] R. Hiptmair and C. Schwab. "Natural boundary element methods for the electric field integral equation on polyhedra". In: *SIAM J. Numer. Anal.* 40.1 (2002), pp. 66–86. ISSN: 0036-1429. DOI: 10.1137/S0036142901387580. URL: https://doi.org/10.1137/S0036142901387580.

[9] Ralf Hiptmair and Lars Kielhorn. *BETL - A generic boundary element template library*. Tech. rep. 2012-36. Switzerland: Seminar for Applied Mathematics, ETH Zürich, 2012. URL: https://www.sam.math.ethz.ch/sam_reports/reports_final/reports2012/2012-36.pdf.

[10] Lucy Weggler. "High order boundary element methods". Universität des Saarlandes, Jan. 2011. DOI: 10.22028/D291-26256.

[11] Lucy Weggler. "Stabilized boundary element methods for low-frequency electromagnetic scattering". In: *Math. Methods Appl. Sci.* 35.5 (2012), pp. 574–597. ISSN: 0170-4214. DOI: 10.1002/mma.1597. URL: https://doi.org/10.1002/mma.1597.

8 Appendix

8.1 Mie Solution

A well known study case for electromagnetic scattering is the one of a spherical conductor hit by a plane wave. We consider a PEC sphere, although the solution is known also for the case of with finite conductivity. The solution is valid only for an incident wave with polarization $\mathbf{d} = [0, 0, -1]^T$ and direction $\mathbf{p} = [1, 0, 0]^T$.
The expression of the incident electric field associated with the plane wave is

$$\mathbf{E}^i = \mathbf{p} e^{i\kappa \mathbf{x}\cdot\mathbf{d}}.$$

Moreover, by formal computation it can be shown that

$$\mathbf{curl}\ \mathbf{E}^i = i\kappa \mathbf{d} \times \mathbf{E}^i,$$

which is useful to compute the Neumann trace of the plane wave. The scattered field is

$$\mathbf{E}^s = \sum_{n=1}^{\infty} i^n \frac{2n+1}{n(n+1)} (a_n \mathbf{m}_{o1n}^{(3)} - i b_n \mathbf{n}_{e1n}^{(3)})$$

and

$$\mathbf{curl}\ \mathbf{E}^s = i\kappa \sum_{n=1}^{\infty} i^n \frac{2n+1}{n(n+1)} (i a_n \mathbf{n}_{o1n}^{(3)} + b_n \mathbf{m}_{e1n}^{(3)})$$

where

$$a_n = -\frac{j_n(\rho)}{h_n^{(1)}(\rho)}, \quad b_n = -\frac{[\rho j_n(\rho)]'}{[\rho h_n^{(1)}(\rho)]'},$$

$$\mathbf{m}_{e1n}^{(3)} = -\frac{1}{\sin\theta} h_n^{(1)}(\kappa R) P_n^1(\cos\theta) \sin\phi\ \mathbf{e}_2 - h_n^{(1)}(\kappa R) \frac{\partial P_n^1}{\partial \theta}(\cos\theta) \cos\phi\ \mathbf{e}_3,$$

$$\mathbf{n}_{o1n}^{(3)} = \frac{n(n+1)}{\kappa R} h_n^{(1)}(\kappa R) P_n^1(\cos\theta) \sin\phi\ \mathbf{e}_1 + \frac{1}{\kappa R} [\kappa R h_n^{(1)}(\kappa R)]' \frac{\partial P_n^1}{\partial \theta}(\cos\theta) \sin\phi\ \mathbf{e}_2 + \frac{1}{\kappa R \sin\theta} [\kappa R h_n^{(1)}(\kappa R)]' P_n^1(\cos\theta) \cos\phi\ \mathbf{e}_3,$$

$$\mathbf{m}_{o1n}^{(3)} = \frac{1}{\sin\theta} h_n^{(1)}(\kappa R) P_n^1(\cos\theta) \cos\phi\ \mathbf{e}_2 - h^{(1)}(\kappa R) \frac{\partial P_n^1}{\partial \theta}(\cos\theta) \sin\phi\ \mathbf{e}_3,$$

$$\mathbf{n}_{e1n}^{(3)} = \frac{n(n+1)}{\kappa R} h_n^{(1)}(\kappa R) P_n^1(\cos\theta) \cos\phi\ \mathbf{e}_1 + \frac{1}{\kappa R} [\kappa R h_n^{(1)}(\kappa R)]' \frac{\partial P_n^1}{\partial \theta}(\cos\theta) \cos\phi\ \mathbf{e}_2 - \frac{1}{\kappa R \sin\theta} [\kappa R h_n^{(1)}(\kappa R)]' P_n^1(\cos\theta) \sin\phi\ \mathbf{e}_3,$$

$$\rho = \kappa a,$$

a is the radius of the sphere, (R, θ, ϕ) are the spherical coordinates, j_n is the n-th order spherical Bessel function, $h_n^{(1)}$ is the n-th order Henkel function of the first kind and $(\mathbf{e}_1, \mathbf{e}_2, \mathbf{e}_3)$ is the standard basis of $\mathbb{R}^3$.

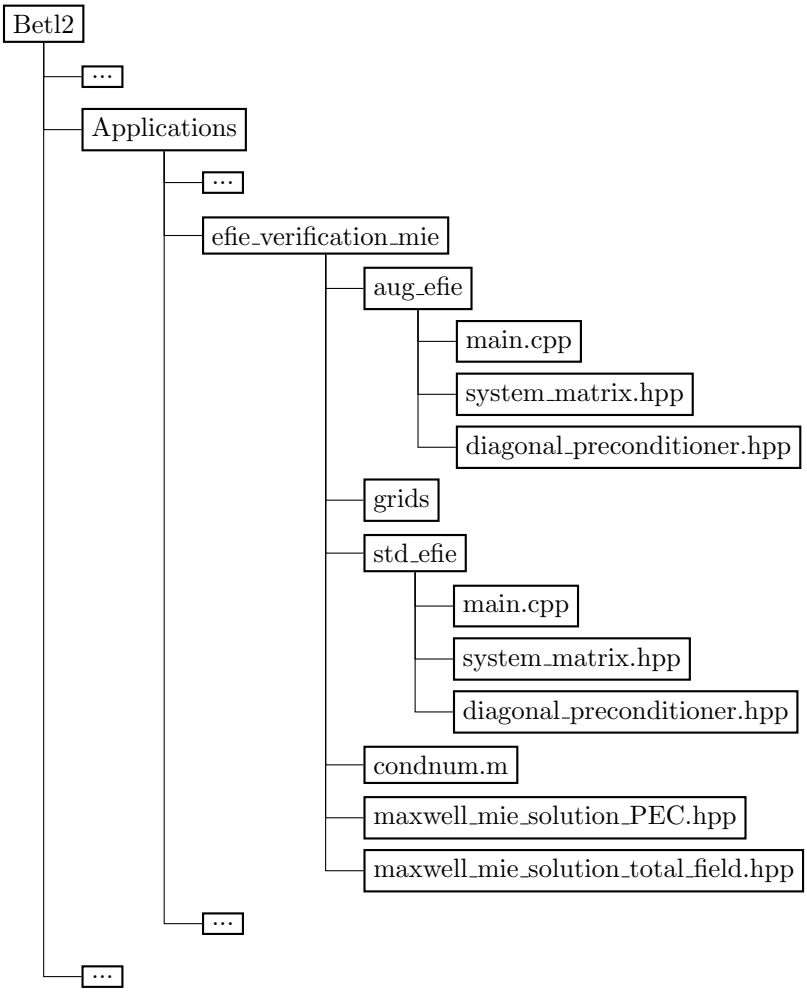

Fig. 5: Structure of Betl2 Gitab repository

8.2 GitLab Repository

In this appendix we describe the structure of our GitLab repository.
The principal folder of our application can be found following the path

Betl2/Applications/efie_verification_mie,

as depicted in figure 5. In this folder we find the sub-folders aug_efie and std_efie corresponding to the two versions implemented. Moreover, we have some common files which are used by both of the versions:

- the grids folder, which contains the meshes for the sphere and the cube used to obtain our numerical results;
- the C++ header file maxwell_mie_solution_PEC.hpp, containing the class in which we implemented the Mie Solution for a PEC sphere;
- the C++ header file maxwell_mie_solution_total_field.hpp, which contains an auxiliary class to return the sum of a plane wave (implemented in

Betl2/Library/analytical_functions/maxwell_plane_wave.hpp) and the Mie Solution for a PEC sphere;

- the Matlab script condnum.m, which allows to compute the condition number of the two versions of the discretized EFIE;

The std_efie and aug_efie directories have the same structure. They contain:

- the main.cpp;
- the system_matrix.hpp header which contains the class for the assembly of the linear system induced by the BEM discretization;
- the diagonal_preconditioner.hpp header which contains a class for a simple preconditioner used in the solution of the linear system;

The symmetry in the structure of these two folders means that probably we could have implemented the application using C++ abstract classes and allowing code reuse.